Fluid Mechanics
in
the anterior- and vitreous chamber of the eye

Jan O. Pralits

Department of Civil, Chemical and Environmental Engineering
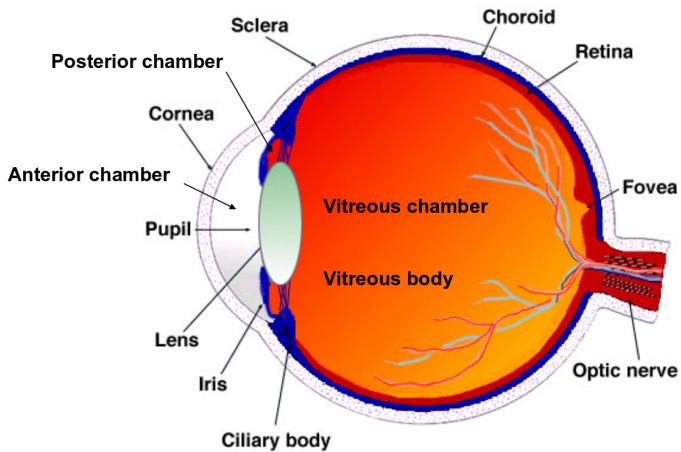University of Genoa, Italy
jan.pralits@unige.it

October 20, 2015

The work presented has been carried in collaboration with:

- **Rodolfo Repetto** DICCA, University of Genoa, Italy;
- **Krystyna Isakova, Peyman Davvalo Khongar, Damiano Natali**
  DICCA, University of Genoa, Italy;
- **Jennifer Siggers** Imperial College London, UK;
- **Mario Romano** Department of Neurosciences, University of Naples Federico II, Italy
- **Tom Williamson** St Thomas Hospital, London, UK
- **Jan-Willem Beenakker** Department of Radiology, Leiden University Medical Center, Leiden, The Netherlands
- **Paolo Soleri** Ophtec BV, The Netherlands

Anatomy of the eye

Anterior chamber I

Flow mechanisms

Flow induced by aqueous production/drainage:
Aqueous humor is produced by the ciliary body, and then flows through the posterior chamber, the pupil and the anterior chamber, from where it is drained into the trabecular meshwork. (3 $\mu l/min$)
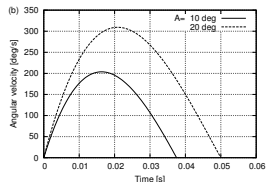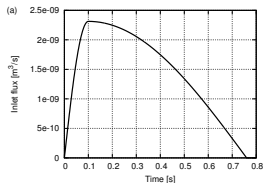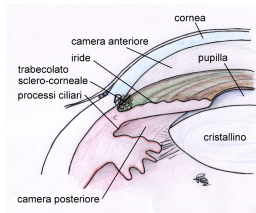
Flow induced during myosis/mydriasis:
During pupil contraction (myosis), a flow from the posterior to the anterior chamber of the eye is generated, which is intense, although it only lasts a short time, typically less than 1 s. (**middle figure**)

Buoyancy-driven flow:
It is well known that, since the posterior surface of the cornea is typically cooler than the iris and lens. We prescribed a temperature of 34 $^{\circ}$C on the cornea and 37 $^{\circ}$C on all other surfaces.
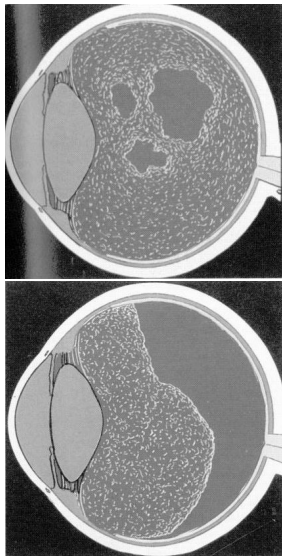
Flow induced by saccades of the eye:
We consider the flow generated in the anterior chamber by rotations of the eye bulb by modeling isolated rotations using the analytical relationship proposed by Repetto et al. (2005) which provides the angular velocity of the eye as a function of time. (**bottom figure**)
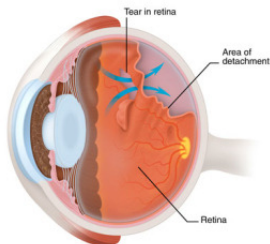
Vitreous ageing

With advancing age the vitreous typically undergoes significant changes in structure.

- Disintegration of the gel structure which leads to **vitreous liquefaction (synchisys)**. This leads to an approximately linear increase in the volume of liquid vitreous with time. Liquefaction can be as much extended as to interest the whole vitreous chamber.

- Shrinking of the vitreous gel **(syneresis)** leading to the detachment of the gel vitreous from the retina in certain regions of the vitreous chamber. This process typically occurs in the posterior segment of the eye and is called **posterior vitreous detachment (PVD)**. It is a pathophysiologic condition of the vitreous.

Retinal detachment

Posterior vitreous detachment (PVD) and vitreous degeneration:

- more common in myopic eyes;
- preceded by changes in vitreous macromolecular structure and in vitreoretinal interface → possibly mechanical reasons.
- If the retina detaches from the underlying layers → loss of vision;

Rhegmatogeneous retinal detachment:

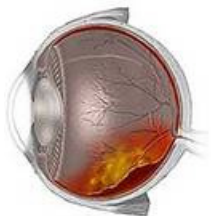- fluid enters through a retinal break into the sub retinal space and peels off the retina.

Risk factors:

- **myopia;**
- posterior vitreous detachment (PVD);
- lattice degeneration;
- ...

Scleral buckling and vitrectomy
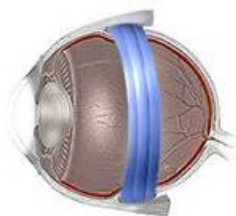
Scleral bluckling

Before   After

Scleral buckling is the application of a rubber band around the eyeball at the site of a retinal tear in order to promote reachtachment of the retina.

Vitrectomy

The vitreous may be completely replaced with tamponade fluids: silicon oils, water, gas, ..., usually immiscible with the eye's own aqueous humor

Investigations

Computer modeling of rhegmatogenous retinal detachment

D. Natali[1], R. Repetto[1], J. O. Pralits[1],
J. H. Siggers[2] and Tom H. Williamson[3]

[1] Department of Civil, Chemical and Environmental Engineering, University of Genoa, Italy,
[2] Department of Bioengineering, Imperial College London, London SW7 2AZ, UK,
[3] Retina Surgery, 50-52 New Cavendish Street, London W1G 8TL, United Kingdom

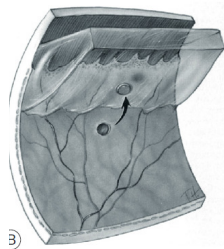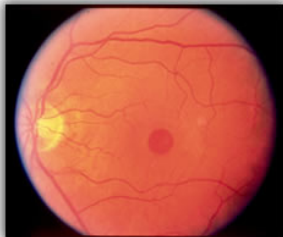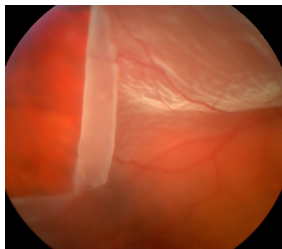A paper is in preparation for *Investigative Ophtamology & Visual Science (IOVS)*

Retinal break

Rhegmatogenous retinal detachment

- Occurs in approximately **1 in 10,000** of the population.
- Caused by the appearance of retinal **breaks in the peripheral retina**
- Unchecked retinal detachment is a **blinding condition**
- There is uncertainty surrounding the mechanism of action of surgical methods.
- **Traction on the retina** from separation of the vitreous is thought to create the retinal break
- Postulated that **saccadic eye movements** create liquefied vitreous flow in the eye, which help to lift the retina.
- Experience says that the **hole** condition detaches quicker than the **free flap** condition

Here: use numerical simulations (**FSI**) to investigate the two cases under realistic conditions to give indications to surgeons.

The retinal detachment: cases considered here

left) (GRT) Giant Retinal Tear (when large, $>90°$), middle) macular hole, right) retinal hole

The retinal detachment: cases considered here

Giant Retinal Tear (GRT)

A   A

Retinal surface

GRT

retinal hole

A   A

Retinal surface

Hole

Section A-A

Eye wall

Retinal flap

Liquified vitreous

Section A-A

Eye wall

Detached retina   Liquified vitreous

Governing equations

For the viscous incompressible fluid
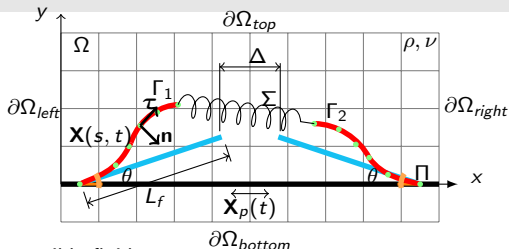
$$\begin{cases} \dfrac{\partial \mathbf{u}}{\partial t} + \mathbf{u} \cdot \nabla \mathbf{u} = -\nabla p + \dfrac{1}{Re}\nabla^2 \mathbf{u} + \mathbf{f} \\ \nabla \cdot \mathbf{u} = 0 \end{cases} ,$$

Periodicity is imposed at $\partial\Omega_{left}$ and $\partial\Omega_{right}$, and symmetry at $\partial\Omega_{top}$ and $\partial\Omega_{bottom}$. Non slip boundary conditions are imposed on solid surfaces.

For the slender 1D structure

$$\frac{\partial^2 \mathbf{X}}{\partial t^2} = \frac{\partial}{\partial s}\left(T\frac{\partial \mathbf{X}}{\partial s} \right) - \frac{\partial^2}{\partial s^2}\left(\gamma \frac{\partial^2 \mathbf{X}}{\partial s^2} \right) + Fr\mathbf{g} - \mathbf{F}$$

The structure is clamped at a certain angle θ at the wall, which moves according to $\mathbf{X_p(t)}$. Incompressibility of the structure is imposed and non-slip/no penetration of the fluid is enforced.

Dimensionless parameters

The governing equations can be non-dimensionalized with the following characteristic scales:
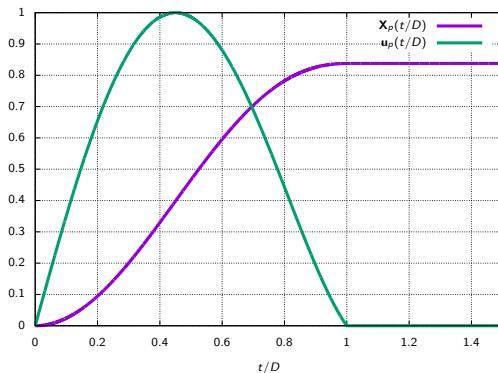
$$x = \frac{x^*}{L^*}, \quad \mathbf{u} = \frac{\mathbf{u}^*}{U_\infty^*}, \quad \mathbf{f} = \frac{\mathbf{f}^* L^*}{\rho_0^* U_\infty^{*2}}, \quad \mathbf{F} = \frac{\mathbf{F}^* L^*}{\rho_1^* U_\infty^{*2}}$$

Doing so, several dimensionless parameters arises:

$$Re = \frac{U_\infty^* L^*}{\nu^*}, \quad Fr = \frac{g^* L^*}{U_\infty^{*2}}, \quad \rho = \frac{\rho_1^*}{\rho_0^* L^*}, \quad \gamma = \frac{K_b^*}{\rho_1^* U_\infty^{*2} L^{*2}}$$

Plate imposed motion

We model isolated rotations using the analytical relationship proposed by Repetto et al. (2005).

- The angle is $8°$
- The maximum velocity is 0.061 m/s
- The duration is 0.045 s
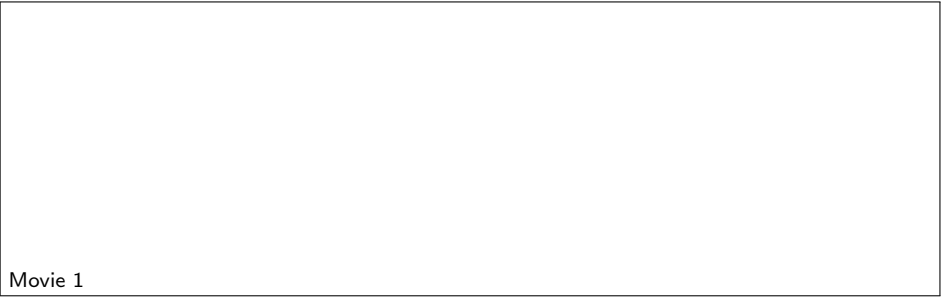
Parameters used in the computations

Quantity	Value	Reference
Properties of the retinal flap		
Density ρ_S	1300 kg/m^3	
Length L	$1.5 - 2.5$ mm	
Thickness	70 μm	Alamouti and Funk (2003), Foster et al. (2010), Ethier et al. (2004), Bowd et al. (2000), Wollensak and Eberhard (2004), Dogramaci and Williamson (2013)
Bending stiffness K_b	$2.98 \cdot 10^{-11}$ Nm^2	$Eh^3/12$
Young's modulus E	$1.21 \cdot 10^3$ N/m2	Jones et al. (1992), Wollensak and Eberhard (2004), Reichenbach et al. (1991), Sigal et al. (2005)
Properties of the fluid		
Density ρ_F	1000 kg/m^3	Foster et al. (2010)
Dynamic viscosity μ	$1.065 \cdot 10^{-3}$ kg/ms	Foster et al. (2010)

Table: Parameter values used for the simulations and corresponding references when available.

Dynamics for retinal tear

L=2 mm, $\theta = 33.6°$

Movie 1

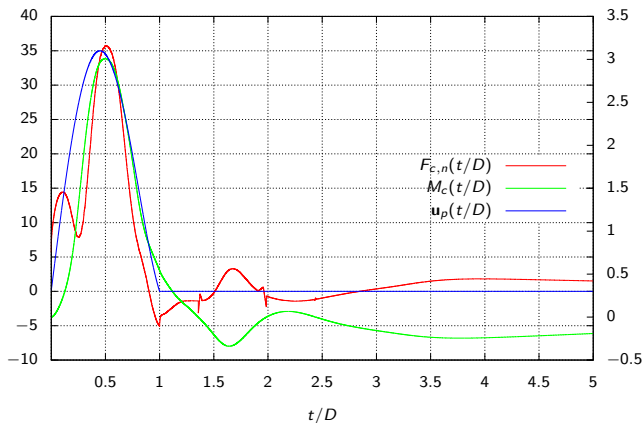# Dynamics for retinal hole

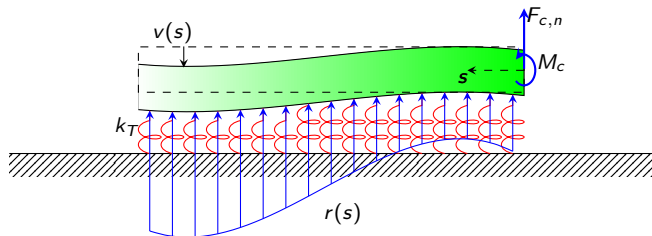L=2 mm, $\theta = 33.6°$, $\Delta = 0.17$ mm

Movie 2

Clamping force and torque evaluation

We evaluate the wall-normal force ($F_{c,n}$) and torque (M_c) at the clamping point as a function of time. These values are then used to model the **tendency to further detach**.

Winkler theory

Semi-infinite foundation (in green) subject to a punctual force $F_{c,n}$ and torque M_c at the finite end, and supported by elastic springs of stiffness k_T (in red). The soil reaction $r(s)$ (in blue) is proportional to the foundation displacement $v(s)$.
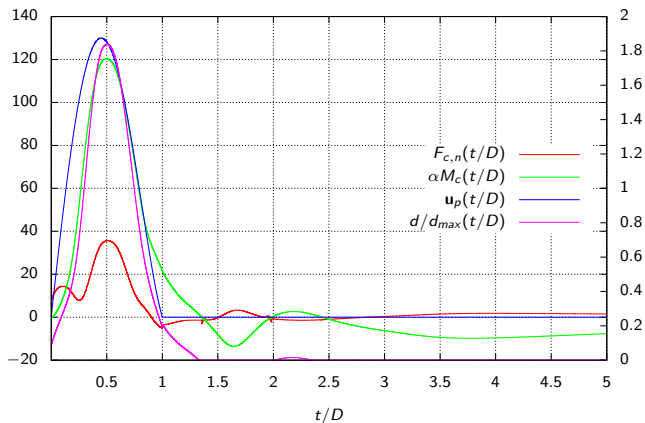
$$v(s) = \frac{e^{-\alpha s}}{2\alpha^3 \gamma} \{\alpha M_c [\cos(\alpha s) - \sin(\alpha s)] + F_{c,n} \cos(\alpha s)\},$$

$$d = \max(v|_{s=0}, 0) = \max(\frac{\alpha M_c + F_{c,n}}{2\alpha^3 \gamma}, 0),$$

where α is the ratio between the soil spring rigidity k_T and the foundation beam stiffness γ.

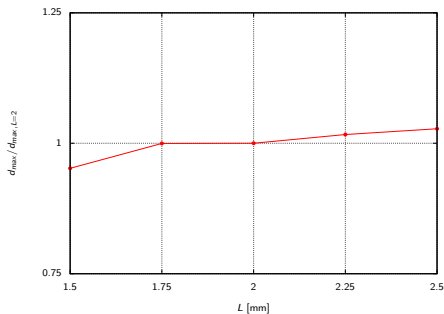### d is the tendency to detach

Tendency to detach

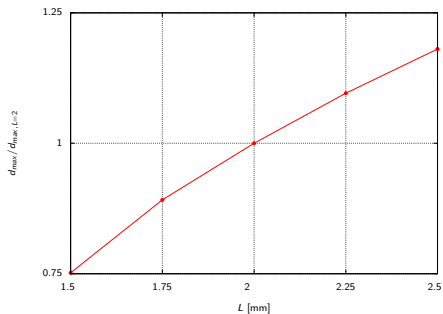d attains a maximum value for a finite value of t/D

Different filament lengths L: maximum tendency to detach

clamping angle $\theta = 33.56°$, $\Delta = 0.17mm$ (retinal hole)

Tear

Hole

Increasing L increases the maximum value of d

Different clamping angles θ: maximum tendency to detach

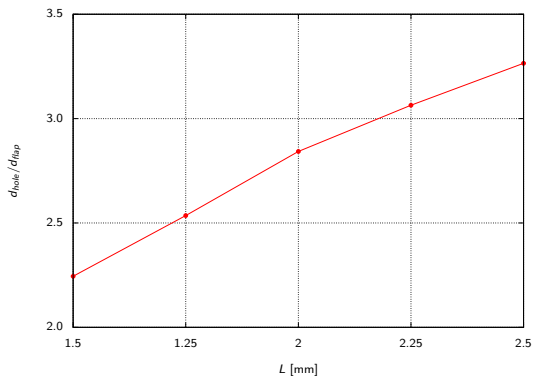length $L = 2$ mm, $\Delta = 0.17mm$ (retinal hole)

Tear

Hole

A maximum value of d is found

Comparison horseshoe tear & hole: maximum tendency to detach

clamping angle $\theta = 33.56°$, $\Delta = 0.17mm$ (retinal hole)

The retinal hole is more prone to detach compared to horseshoe tear

Conclusions

The tendency to detach has been analyzed both for the **free flap** and **hole case** for different values of the detached retinal length, clamping angle and inter-tip distance (in the case of retinal hole). The general conclusions can be summarized as follows:

- The tendency to detach of a retinal hole, compared to a retinal free flap, is 2 - 3 times larger for retinal filaments of 1.5 - 2.5 mm, with increasing values of d for increasing values of the filament length.
- The tendency to detach increases as the retinal filament length increases, both for the retinal hole- and retinal free flap case.
- A worst-case angle is found when the tendency to detach is investigated for different clamping angles. The value is $\simeq 25°$ in the free flap case and $\simeq 34°$ in the hole case.
- The effect of changing the inter-tip distance, which is related to the size of the retinal hole, on the tendency to detach is weak.

Ongoing: experimental setup of **retinal hole** to understand **three-dimensional effects**, with **Christophe Clanet, Martin Coux, Zhexin Pan**

A model for the linear stability of the interface between aqueous humor and vitreous substitutes after vitreoretinal surgery

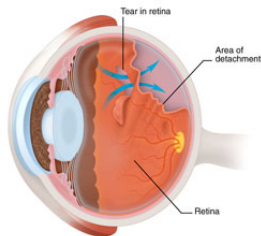K. Isakova[1], J. O. Pralits[1], R. Repetto[1], M. R. Romano[2]

[1] Department of Civil, Chemical and Environmental Engineering, University of Genoa, Italy,
[2] Istituto Clinico Humanitas, Milano, Italy

Stability of the interface between aqueous humor and vitreous substitutes after vitreoretinal surgery

Retinal detachment

Warning signs of retinal detachment:

- Flashing lights.
- Sudden appearance of floaters.
- Shadows on the periphery of your vision.
- Gray curtain across your field of vision.

Vitrectomy

The vitreous may be completely replaced with tamponade fluids: silicon oils, air, gas, ...

- Denoted **tamponade liquids**
- Purpose: Induce an instantaneous interruption of an open communication between the subretinal space/retinal pigment epithelial cells and the pre-retinal space.
- Healing: a scar should form as the cells absorb the remaining liquid.

Fluids commonly used as a vitreous substitutes

- **Silicone oils**;
  - $960 \leq \rho^* \leq 1290$ kg/m^3
  - $10^{-4} \leq \nu^* \leq 5 \times 10^{-3}$ m/s^2
  - $\sigma^* \approx 0.05$ N/m

- **Perfluorocarbon liquids**;
  - $1760 \leq \rho^* \leq 2030$ kg/m^3
  - $8 \times 10^{-7} \leq \nu^* \leq 8 \times 10^{-6}$ m/s^2
  - $\sigma^* \approx 0.05$ N/m

- **Semifluorinated alkane liquids**;
  - $1350 \leq \rho^* \leq 1620$ kg/m^3
  - $4.6 \times 10 \leq \nu^* \leq 10^{-3}$ m/s^2
  - $0.035 \leq \sigma^* \leq 0.05$ N/m

The choice of tamponade liquid depends on the specific case

- The tabulated fluids are **immiscible** with water and commonly used in surgery
- A lighter fluid (cf. water) is used to tamponade in the upper part
- A heavier fluid is used to tamponade in the lower part
- High surface tension is preferred to a low value (**EXPERIENCE**)
- High value of viscosity (cf. water) is preferred to a low value (**EXPERIENCE**)

What could happen otherwise ?

Emulsification

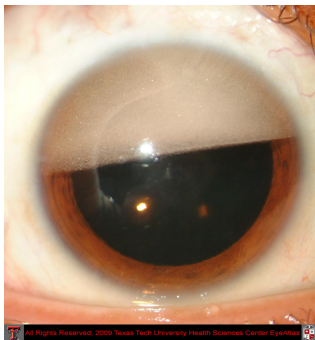Emulsification leads to loss of vision, **not satisfactory**

Figure: Emulsification (inverted hypopyon) of vitreous substitutes in the vitreous chamber
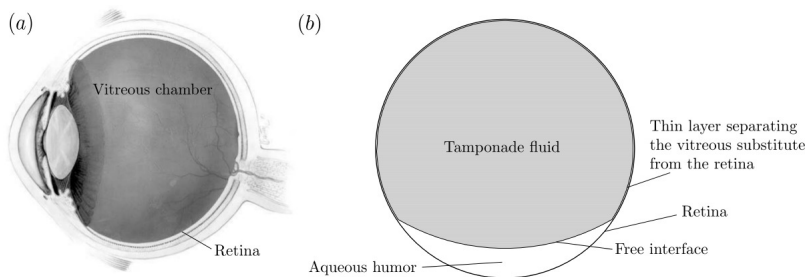
Summary & Motivation

Summary

- From **experience** it is known that tamponade fluids with **high surface tension** and **high viscosity** (compared to water) are less prone to emulsify
- It is also know that initially "good" tamponade fluids tend to change with time, for instance a decrease of surface tension due to **surfactants**, which leads to emulsification.
- It is generally believed that **shear stresses** at the tamponade fluid-aqueous **interface** generated during eye rotations play a crucial role in the generation of an emulsion.
- The tamponade liquid needs to stay for a period of months so it is of interest to know how emulsification can be avoided.

Our analysis

- We want to understand how emulsification, or the initial stages leading to emulsification, are related to the parameters (surface tension, viscosity, density, real conditions).
- As a first study we focus on the **stability characteristics of the interface** in order to see if it has any role.
- A linear stability analysis, of wave like solutions, is used.
- The evolution of the disturbance kinetic energy is analyzed.

Mathematical model I

The geometry

(a) Vitreous chamber, Retina

(b) Tamponade fluid, Thin layer separating the vitreous substitute from the retina, Retina, Free interface, Aqueous humor

Mathematical model II
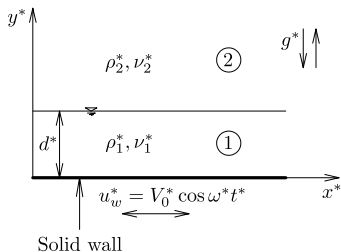
Underlying assumptions

Figure: Geometry of the problem

- $d^* << R^*$
- 2D-model;
- flat wall oscillating harmonically;
- semi-infinite domain;
- small perturbations;
- quasi-steady approach.
- Stokes problem when $\{\}_1 = \{\}_2$

Scaling and Dimensionless Parameters

$$\mathbf{x} = \frac{\mathbf{x}^*}{d^*}, \quad \mathbf{u_i} = \frac{\mathbf{u_i}^*}{V_0^*}, \quad p_i = \frac{p_i^*}{\rho_1^* V_0^{*2}}, \quad t = \frac{V_0^*}{d^*} t, \quad \omega = \frac{d^*}{V_0^*} \omega^*$$

$$m = \frac{\mu_2^*}{\mu_1^*} \qquad\qquad\qquad \gamma = \frac{\rho_2^*}{\rho_1^*}$$

$$Re = \frac{V_0^* d^*}{\nu_1^*} \qquad\qquad\qquad Fr = \frac{V_0^*}{\sqrt{g^* d^*}}$$

$$S = \frac{\sigma^*}{\rho_1^* d^* V_0^{*2}} = \frac{1}{We}$$

Basic flow

Analytical solution

Parallel time-dependent flow

$$U_1(y, t) = (c_1 e^{-ay} + c_2 e^{ey}) e^{i\omega t} + c.c.,$$

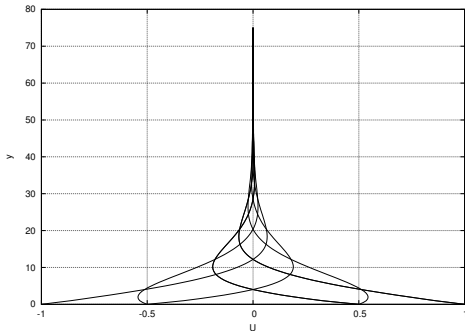$$U_2(y, t) = c_3 e^{-by} e^{i\omega t} + c.c.,$$

$$\frac{\partial P_1}{\partial y} = -Fr^{-2},$$

$$\frac{\partial P_2}{\partial y} = -\gamma Fr^{-2},$$

where

$$a = \sqrt{i\omega R}, \qquad b = \sqrt{\frac{i\gamma\omega R}{m}}.$$

and c_1, c_2, c_3 are functions of a, b, m.

Linear stability analysis

Flow decomposition:

$$u_i = U_i + u_i', \ v_i = v_i' \quad p_i = P_i + p_i'$$

Boundary conditions:

$$u_1'(0, t) = v_1'(0, t) = 0 \quad \text{and} \quad u_2'(y, t) \to 0, \ v_2'(y, t) \to 0 \quad \text{as} \quad y \to \infty$$

Interface: $(y^* = d^*)$ introducing also the perturbation of the interface η'

- Continuity of the perturbation velocity components across the interface
- Continuity of the tangential stress of across the interface
- The wall normal stress is balanced by the surface tension

A quasi-steady approach is assumed with two-dimensional wave-like solutions as:

$$\xi_i = e^{i\alpha(x-\Omega t)}\hat{\xi}_i(y, \tau) + c.c$$

where

$$0 \le \tau \le 2\pi/\omega$$

The system of equations is reduced introducing the perturbation stream function giving **two Orr-Sommerfeld equations**, discretized using finite differences, solved using an inverse iteration algorithm.

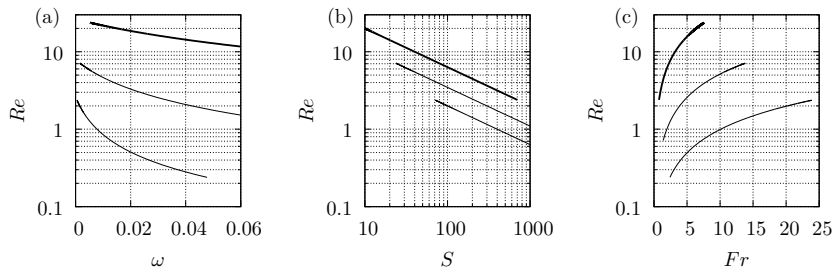# Range of variability of the dimensionless parameters

Figure: Relationship between $Re - \omega$, $Re - S$ and $Re - Fr$ obtained adopting feasible values of eye movement. From thin to thick curves: $d = 1 \times 10^{-5}$m, $d = 3 \times 10^{-5}$m, $d = 1 \times 10^{-4}$m
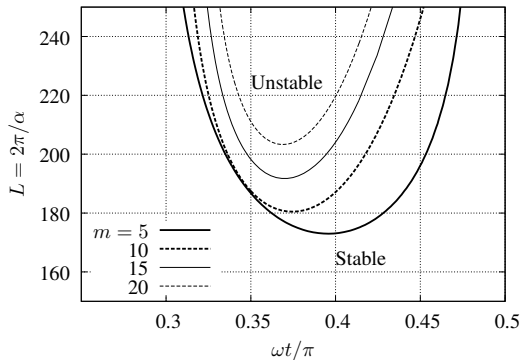
Neutral Curves

Figure: $S = 14$, $\gamma = 1.0$, $Re = 7$, $\omega = 0.001$

Shortes unstable wave length

The **shortest** unstable wave length as a function of S, Re and γ.
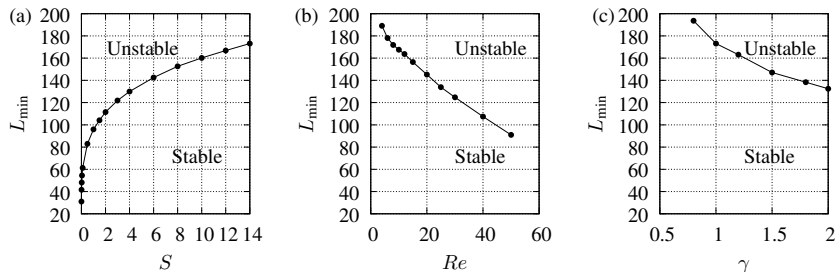

Figure: Length of the shortest unstable perturbation L_{min} versus S (a), Re (b), and γ (c) with $\omega = 0.001$ and $m = 5$. The values of $Re = 7$ in (a) and (c), $S = 14$ in (b) and (c), and $\gamma = 1$ in (a) and (b), respectively.

Conclusions and Continuation

Monitoring the shortest unstable wave length (critical wave length) we have seen that:

- Increasing the viscosity, ratio the critical wave length increases (**stabilizing for the Eye**)
- Increasing the surface tension, the critical wave length increases (**stabilizing for the Eye**)
- Increasing the Reynolds no., the critical wave length decreases (**destabilizing for the Eye**)
- Increasing the density ratio, the critical wave length decreases (**destabilizing for the Eye**)
- The first two is "in line" with realistic observations.
- For realistic values of $R, S, \gamma, m, \omega, d^*$ the critical wave length $\approx$ 5 mm, which is about half the Eye radius.
- However, the growth rate is instantaneous and the waves unstable only during certain intervals of one period. (cf. turbulent burst in the classical Stokes II problem). No sustained growth over one period is guaranteed.
- This analysis is far from explaining the onset of emulsion but a first step to rule out (or not) different physical mechanisms.

Next step...

- Modal & nonmodal analysis using cylindrical shape in collaboration with **Lutz Lesshafft** & **Onofrio Semeraro**
- Physical understanding of emulsification with **Charles Baroud**

Equilibrium shape of the aqueous humour-vitreous substitute interface

K. Isakova[1], J. O. Pralits[1], M. R. Romano[2], J.-W. Beenakker[3] and R. Repetto[1]

[1] Department of Civil, Chemical and Environmental Engineering, University of Genoa, Italy
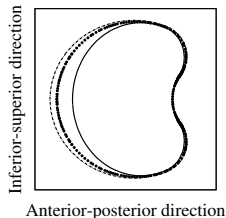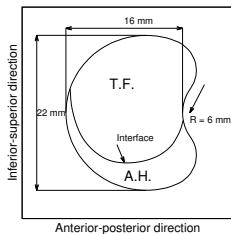[2] Istituto Clinico Humanitas, Milano, Italy
[3] Leiden University, Netherlands,

A paper is in preparation for *investigative ophtamology & visual science (iovs)*

Equilibrium shape

Tamponade fluids (TF) used for vitrectomy are immiscible with aqueous humor (AH) and a small pocket of AH is therefore created between the TF and the retina. Knowing the shape of the interface and where the TF is in contact with the retina is **important information for the surgeons**.

The purpose here is to **predict with a numerical model the shape of the interface between aqueous humor and tamponade fluids** in the vitreous chamber, in the case of use of a gas or a silicon oil. To determine the retinal coverage in the case of various eye shapes, from **normal** to highly **myopic eyes**.
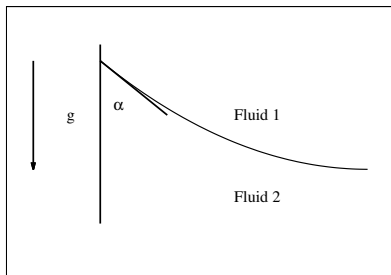

The eye geometry has been taken from Atchison and Smith (2000) and the myopic eye is elongated in all directions and dimensions are taken from Atchison et al. (2004).

Mathematical model

From the Laplace-Young equation

$$2k_m = -\frac{\Delta \rho g}{\gamma} y_i + B,$$

we see that the interface y_i depends on the **density difference** $\Delta \rho$, **surface tension** γ. The constant B can be found imposing the **contact angle** α at the solid boundary.

Mechanical properties of tamponade fluids

In this study we analyze both gas and silicone oil, both used in sugary, with values taken from the literature.

Fluid	Density (kg/m^3)	Surface tension with aqueous (N/m)	Contact angle with the retina (deg)
Silicone oil	980	0.044	16.17 ± 1.23
Intraocular gas	≈ 1	0.07	30.74 ± 4.24
Aqueous humour	1000	-	-

Numerical model

The numerical, thee-dimensional steady solution is obtained using the OpenFOAM, in particular

- VoF method: to keep track of the liquid-liquid interface or gas-liquid interface

- snappyHexMesh: to generate the mesh (not efficient but simple)

- a normal mesh has about 1.7M volumes and we run a a 32 processor work station

- we integrate the governing equations in time and "tune" the viscosity for numerical efficiency

Validation of the numerical model

The numerical code was first validated for the case of sphere by comparing the results with those obtained by solving, analytically, the Laplace–Young equation.
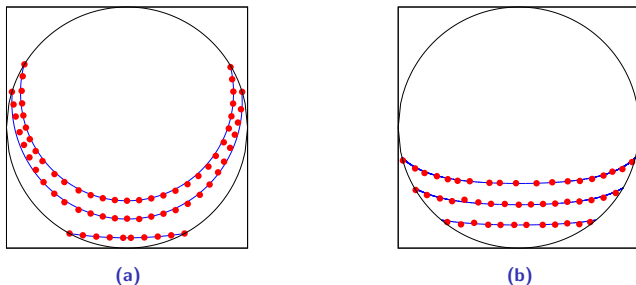

(a)   (b)

Figure: Shape of the interface in the spherical domain computed by analytical model (lines) and by the numerical model (dots) for different volume fraction of tamponade fluids: silicone oil (a) and intraocular gas (b).

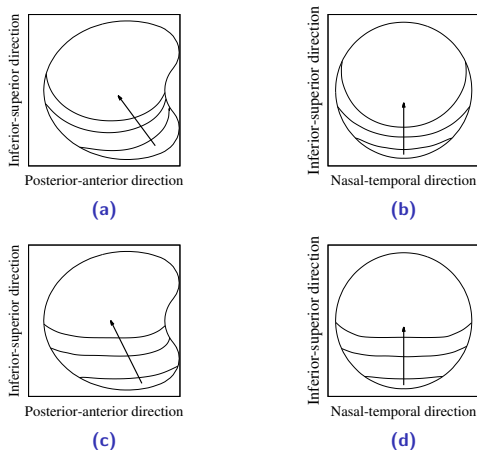# Results I

Emmetropic eyes (model geometry)

Figure: Interface in the normal eye for the silicone oil (a)-(b) and gas (c)-(d). Three different degrees of filling - 90%, 75% and 60%. The arrows indicate decreasing values of $V_{\text{T.F.}}/V$.

Results II

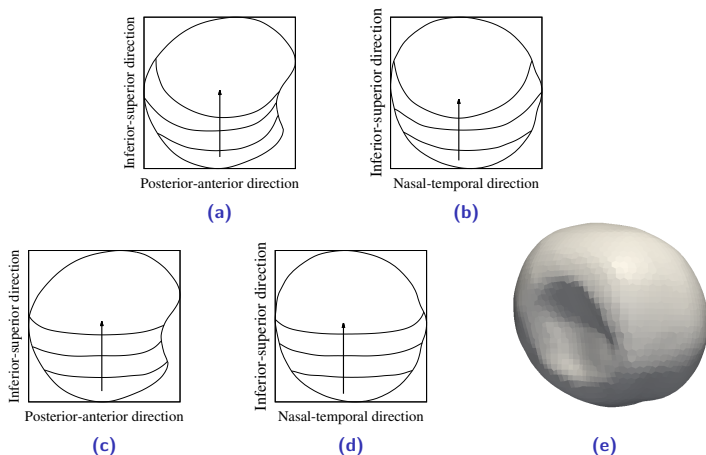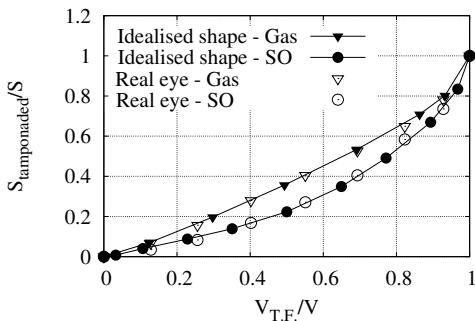**Emmetropic eyes (real eye from MRI)**

Figure: Equilibrium shapes of the interface in the real eye domain for the SO (a,b) and gas (c,d). MRI of the real eye (e). The degrees of filling - 90%, 75% and 60%. The arrows indicate decreasing values of $V_{\mathrm{T.F.}}/V$.

Results III

Relative tamponaded surface

(a)

Figure: Relative tamponaded surface as a function of the volume fraction for the case of SO and gas. Solid symbols refer to the idealized shapes of the vitreous chamber and open symbols to a real, reconstructed eye.
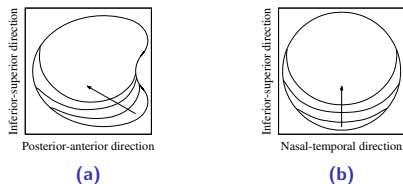
Results IV

Myopic eyes (model geometry)

(a)
(b)

Figure: Interface in the myopic eye for the silicone oil. Axial length is 26.6 *mm*, height and width are 22.75 *mm*.
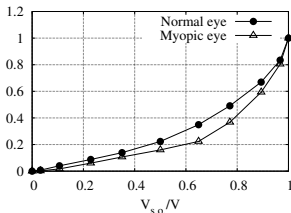

Figure: Relative tamponated surface as a function of the volume fraction for an emmetropic and a highly myopic eye, in the case of SO. The axial length is 24.6 mm.

Results V

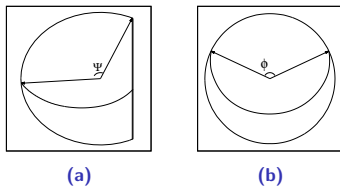## Comparison normal and myopic eyes (angle)

(a)   (b)

Figure: Coverage angles Ψ and Φ. In figure (a) we show the way we measure the coverage angle Ψ on the antero-posterior cross-section and in figure (b) the angle Φ on the equatorial plane.
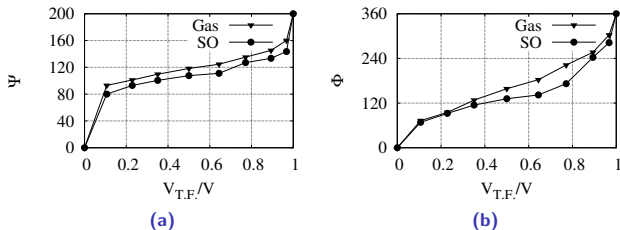

(a)   (b)

Figure: Coverage angles Ψ and Φ in degrees versus the filling ratio $V_{\text{T.F.}}/V$ in the case of SO and gas.

Phakic iris-fixated intraocular lens placement in the anterior chamber: effects on aqueous flow

R. Repetto[1], J. O. Pralits[1], J. H. Siggers[2] and P. Soleri[3]

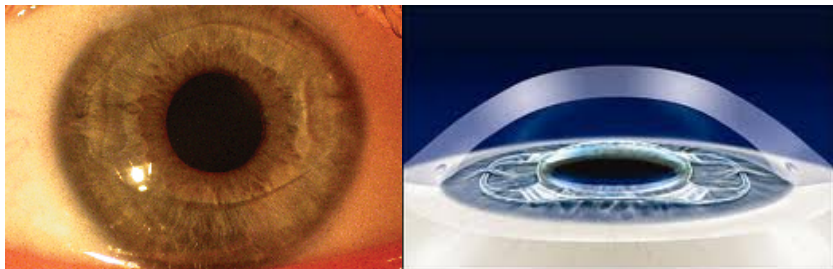[1] Department of Civil, Chemical and Environmental Engineering, University of Genoa, Italy,
[2] Department of Bioengineering, Imperial College London, London SW7 2AZ, UK,
[3] Ophtec BV, Schweitzerlaan 15, 9728 NR, Groningen, The Netherlands

Flow of aqueous humour with an intraocular lens

Phakic intraocular lenses

Motivation

Intraocular lenses decrease endothelial cell density in some patients. Possible reasons include:

- Excess shear stress due to altered flow of aqueous
- Impaired transport of nutrients due to altered flow
- Non-ideal placement of lens, with respect to iris and other tissues
- Impact of external body on eye (e.g. accidental impact, patient touching eyes)

This study: Investigate the first possibility, by comparing the shear stress both in the presence of and without the lens. Moreover, monitor the intra-ocular pressure (IOP).

Description of the model

Governing equations:

$$\boldsymbol{\nabla} \cdot \mathbf{u} = 0$$

$$\rho \left(\frac{\partial \mathbf{u}}{\partial t} + \mathbf{u} \cdot \boldsymbol{\nabla} \mathbf{u} \right) = - \boldsymbol{\nabla} p + \nabla^2 \mathbf{u} + \rho \mathbf{g}$$

$$\rho c_p \left(\frac{\partial T}{\partial t} + \mathbf{u} \cdot \boldsymbol{\nabla} T \right) = k_a \nabla^2 T$$

Assumptions:

- Boussinesq approximation (ρ is constant, except in the gravitational acceleration term in which $\rho = \rho_0(1 - \alpha(T - T_0))$)

Numerical solution:

- All solutions are obtained with *OpenFOAM*
- Solvers were first tested on cases where analytical solutions exist.

Definitions:

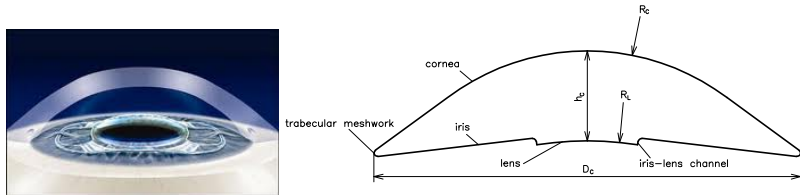| Symbol	Definition
$\mathbf{u}$	velocity
p	pressure
ρ	density of aqueous
μ	viscosity of aqueous
$\mathbf{g}$	acceleration due to gravity
c_p	specific heat at constant pressure
T	temperature
k_a	thermal conductivity of aqueous

Model geometry

Figure: (left) "real" anterior chamber, (right) cross-section of the idealized anterior chamber used in the simulations.
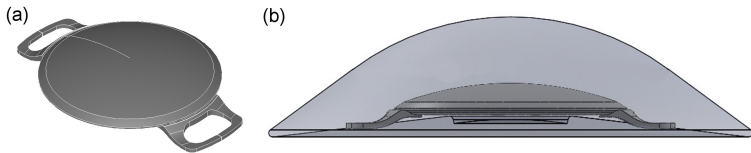

Figure: (a) Geometry of the pIOL consisting of a lens and two haptics that have claws that allow the lens to be attached to the iris, (b) pIOL placed in the anterior chamber.
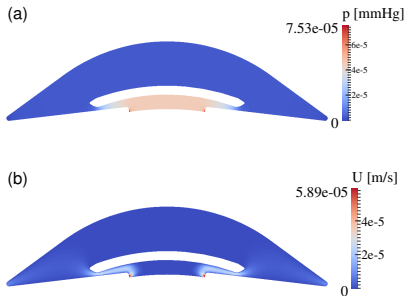
Flow induced by aqueous production and drainage

(a)

p [mmHg]

7.53e-05

0

(b)

U [m/s]

5.89e-05

0

Figure: Flow due to production/drainage of aqueous humor with the device present: (a) excess pressure above IOP, (b) velocity magnitude.
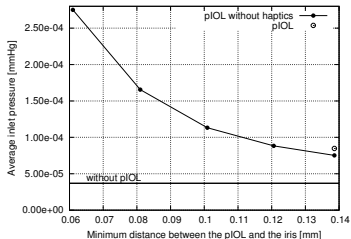

Figure: Average pressure drop between iris–lens channel and trabecular meshwork as a function of the minimum distance between the pIOL and the iris (solid circles). No pIOL (horizontal line) and pIOL with haptics (empty circle).

Lubrication theory:

$$\Delta p = \frac{6\mu Q}{\pi} \int_{r_1}^{r_2} \frac{dr}{rh^3},$$

To get $\Delta p = 1 mmHg$ you need $h = 1\ \mu m$
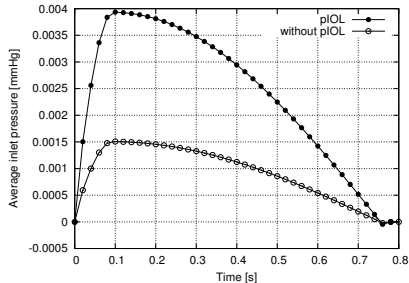
Flow induced during miosis

Figure: Spatially averaged pressure over the inlet as a function of time during miosis, in an eye both with the pIOL (solid circles) and without it (open circles).
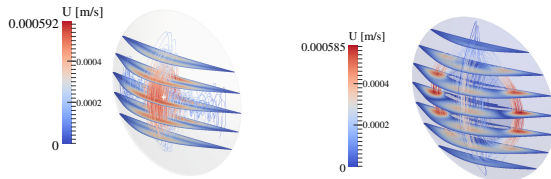
Buoyancy-driven flow I

Figure: Gravity acts in the vertical direction. Streamlines of the flow and the distribution of the velocity magnitude on selected horizontal planes, (a) without the lens, (b) with the lens.
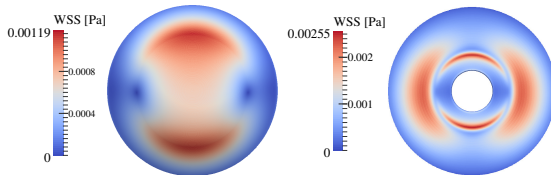

Figure: Buoyancy-driven flow in the presence of the pIOL. (a) Magnitude of WSS on the cornea; (b) WSS on the iris.
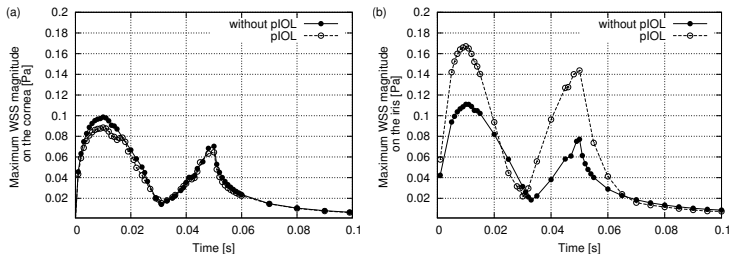
Flow induced by saccades of the eye

Figure: Time evolution of the spatial maximum of the WSS on the (a) cornea and (b) iris in an eye performing a saccade of angle 10 $^\circ$.

Discussion and conclusions

(i) If the lens is properly placed there is a **negligible influence on the pressure** in the posterior chamber.

(ii) There is **no significant increase** of the WSS on the cornea.

(iii) The WSS on the iris is significantly greater than in the case with no pIOL, but the increase is not likely to be sufficiently great so as to give a risk of cell detachment.

Ongoing: Investigating insufficient delivery of oxygen **and/or nutrients** to the corneal epithelium, as a possible cause of epithelium cell loss, together with **Peter Pinsky at Stanford University**.

References I

B. Alamouti and J. Funk. Retinal thickness decreases with age: an oct study. *British Journal of Ophthalmology*, 87(7):899–901, 2003.

D. A. Atchison and G. Smith. *Optics of the human eye*. Butterworth-Heinemann, 2000.

D. A. Atchison, C. E. Jones, K. L. Schmid, N. Pritchard, J. M. Pope, W. E. Strugnell, and R. A. Riley. Eye shape in emmetropia and myopia. *Investigative Ophthalmology & Visual Science*, 45 (10):3380–3386, 2004. doi: 10.1167/iovs.04-0292.

C. Bowd, R. N. Weinreb, B. Lee, A. Emdadi, and L. M. Zangwill. Optic disk topography after medical treatment to reduce intraocular pressure. *American Journal of Ophthalmology*, 130(3): 280 – 286, 2000. ISSN 0002-9394. doi: http://dx.doi.org/10.1016/S0002-9394(00)00488-8. URL http://www.sciencedirect.com/science/article/pii/S0002939400004888.

M. Dogramaci and T. H. Williamson. Dynamics of epiretinal membrane removal off the retinal surface: a computer simulation project. *Br. J. Ophthalmol.*, 97 (9):1202–1207, 2013. doi: 10.1136/bjophthalmol-2013-303598.

C. R. Ethier, M. Johnson, and J. Ruberti. Ocular biomechanics and biotransport. *Annu. Rev. Biomed. Eng.*, 6:249–273, 2004.

W. J. Foster, N. Dowla, S. Y. Joshi, and M. Nikolaou. The fluid mechanics of scleral buckling surgery for the repair of retinal detachment. *Graefe's Archive for Clinical and Experimental Ophthalmology*, 248(1):31–36, 2010.

I. L. Jones, M. Warner, and J. D. Stevens. Mathematical modelling of the elastic properties of retina: a determination of young's modulus. *Eye*, (6):556–559, 1992.

References II

B. Lee, M. Litt, and G. Buchsbaum. Rheology of the vitreous body. Part I: viscoelasticity of human vitreous. *Biorheology*, 29:521–533, 1992.

C. S. Nickerson, J. Park, J. A. Kornfield, and H. Karageozian. Rheological properties of the vitreous and the role of hyaluronic acid. *Journal of Biomechanics*, 41(9):1840–6, 2008. doi: 10.1016/j.jbiomech.2008.04.015.

A. Reichenbach, W. Eberhardt, R. Scheibe, C. Deich, B. Seifert, W. Reichelt, K. Dähnert, and M. Rödenbeck. Development of the rabbit retina. iv. tissue tensility and elasticity in dependence on topographic specializations. *Experimental Eye Research*, 53(2):241 – 251, 1991. ISSN 0014-4835. doi: http://dx.doi.org/10.1016/0014-4835(91)90080-X. URL http://www.sciencedirect.com/science/article/pii/001448359190080X.

R. Repetto, A. Stocchino, and C. Cafferata. Experimental investigation of vitreous humour motion within a human eye model. *Phys. Med. Biol.*, 50:4729–4743, 2005.

I. A. Sigal, J. G. Flanagan, and C. R. Ethier. Factors influencing optic nerve head biomechanics. *Investigative Ophthalmology & Visual Science*, 46(11):4189, 2005. doi: 10.1167/iovs.05-0541. URL +http://dx.doi.org/10.1167/iovs.05-0541.

K. Swindle, P. Hamilton, and N. Ravi. In situ formation of hydrogels as vitreous substitutes: Viscoelastic comparison to porcine vitreous. *Journal of Biomedical Materials Research - Part A*, 87A(3):656–665, Dec. 2008. ISSN 1549-3296.

G. Wollensak and S. Eberhard. Biomechanical characteristics of retina. *Retina*, (24):967–970, 2004.